Thin-airfoil theory applied to hydrofoils with a single finite cavity and arbitrary free-streamline detachment

By A. G. FABULA

U.S. Naval Ordnance Test Station, Pasadena, California

(Received 9 June 1961)

Thin-airfoil theory is applied to steady, plane potential flow about vented or cavitating hydrofoils of arbitrary profile when there are two free-streamlines detaching from the foil and bounding the single cavity that extends downstream of the trailing edge. Cavity-termination models employed are the closed, the partly closed and the open models for which the thickness of the implied 'wake' following the cavity ranges from zero to maximum for the open model. The general solution for given wetted-surface profile, cavity length and particular cavity termination is constructed by superposition of the profile's cusp-closure solution (angle of attack α^+) plus the particular flat-plate solution to give the desired angle of attack α. Four related integrals involving the wetted-surface contour slope distribution lead to drag, lift, cavity pressure and α^+ *vs* cavity length. A comparison of theoretical and experimental lift and drag for a cavitating hydrofoil shows good agreement until the theoretical cavity closure nears the trailing edge.

1. Introduction

The problem considered is steady, plane, irrotational and incompressible flow about a thin hydrofoil, at small angle of attack α, from which free streamlines detach unsymmetrically, as in figure 1. The flow is otherwise unbounded. The

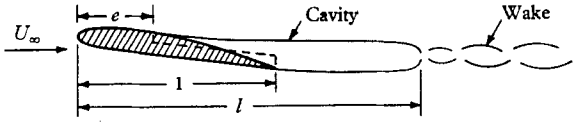

FIGURE 1. Hydrofoil with full side cavity due to ventilation or cavitation.

known free-streamline detachment points are at $x = e$ on the upper side, with $0 \leqslant e < 1$, and at $x = 1$, the trailing edge, on the lower. Unit chord length is assumed throughout. Since gravity is ignored, specification of the 'upper' side as having the more forward detachment is nominal. l is the length from leading edge to cavity termination, where the free streamlines lose their special character. It is assumed that the cavity is fully developed or full, so that $l > 1$.

The application of major interest is the forced-vented hydrofoil on which gas exhaust, from a spanwise slit or row of closely spaced small holes, forces detachment

at the exhaust line. Experiments have shown the stability of such cavity flows and the feasibility of thus producing a significant lift-force change for control purposes by simple gas valving, e.g. on a torpedo (Lang, Daybell & Smith 1959). The same flow geometry can occur with naturally vented surface-piercing hydrofoils, with hydrofoils designed for only vented operation, as suggested by the dashed base contour in figure 1 (Lang 1959) and with cavitating hydrofoils. The same free-streamline model for $l = \infty$ has been applied to steady and unsteady airfoil flows with separated boundary layer by Woods (Thwaites 1960). Since the pressure distribution is not obtained herein, the application to naturally vented and cavitating hydrofoils is possible only when the detachment points are known.

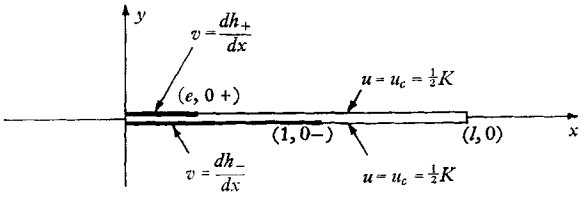

FIGURE 2. Linearized-theory boundary-value problem in physical plane.

By covering the range $0 \leqslant e < 1$, $1 < l \leqslant \infty$, this paper extends previous work for $l = \infty$ with arbitrary e and for arbitrary l with $e = 0$. Trailing-edge venting, $e = 1$, is not included because of a reason evident later and because, for that case, the hydrofoil thickness and camber problems are separable, so that drag, lift and pitching moment are much easier to obtain (Fabula 1960). Also not considered is the so-called partial cavity case with $e < l < 1$, which is usually of less interest. The case of leading-edge detachment, $e = 0$, is naturally included in the present work, but it is not emphasized since that solution is well known in connexion with hydrofoils having a sharp leading edge.

Since most hydrofoils of interest have low thickness ratios a thin airfoil approximation will be used here. This offers considerable simplification in handling the problem of cavity termination as well. In the ordinary linearization with respect to the free-stream speed, U_∞, the total complex velocity is $U + iV = U_\infty(1 + \bar{w})$, where $w = u - iv$ is the desired analytic function of the physical-plane complex variable, $z = x + iy$. The tangency condition for the flow on the upper (+) and lower (−) wetted surfaces is

$$v_\pm = dh_\pm/dx, \tag{1}$$

where $h_\pm(x)$ is the wetted-surface contour.

Cavity pressure is specified by the cavity number

$$K = 2(p_\infty - p_c)/\rho U_\infty^2. \tag{2}$$

Since the linearized Bernoulli equation for the pressure coefficient

$$C_p = 2(p - p_\infty)/\rho U_\infty^2$$

is

$$C_p = -2u, \tag{3}$$

the value of u on the cavity specifies K as

$$K = 2u_{c_{\pm}}. \tag{4}$$

To complete the boundary-value problem, assumptions must be made about free-streamline detachment and cavity termination. The condition of smooth separation is obtained by exluding possible solutions corresponding to certain singularities at the detachment points. Out of a great variety of possible cavity-termination methods, only the closure-singularity method (Tulin 1953) is used. Thus the trailing end of the closed cavity is like the trailing edge of an elliptical-profile airfoil in thin-airfoil theory (Biot 1942). In a minor generalization, the

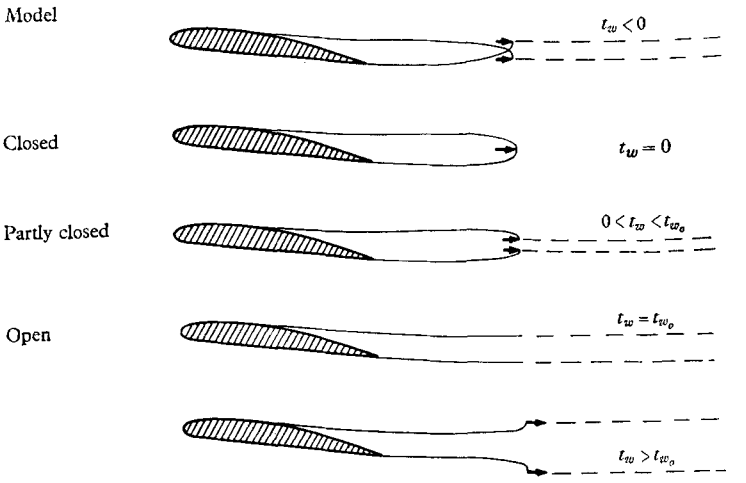

FIGURE 3. Types of cavity termination, according to closure singularity strength, when no singularities are allowed in the wake.

condition of complete cavity closure is relaxed and the 'wake' thickness, t_w, implied by integration of $v(x, 0 \pm)$ over the slit, is allowed to range from zero to t_{w_0}, as in figure 3. Zero wake thickness corresponds to the closed-cavity model, with maximum allowable closure, and maximum wake thickness corresponds to the open-cavity model with zero closure. The point-drag forces at cavity termination, seen in figure 3, are explained later. Of course such crude models of real-fluid wakes are not expected to be accurate, but are merely considered in order to obtain some rough indication of what effects might be expected if experimental wake thickness is found to be appreciable, according to a criterion discussed later.

2. Boundary-value problem in the circle plane

All the single-cavity boundary-value problems discussed here are similar since there is a single portion of the slit periphery on which u is specified. Furthermore, because u is constant in that portion, this simple type of mixed boundary-value problem can be converted into the direct problem of thin-aerofoil theory, whereby

in the 'circle plane', $\zeta(z)$, v is specified on the unit circle, with w less the closure function regular outside the unit circle. Thus for $0 \leqslant e < 1$, $1 < l < \infty$, by use of

$$\zeta = \zeta_1 + i\zeta_2 = \xi + (\xi^2 - 1)^{\frac{1}{2}} \tag{5}$$

with $$\xi = (1+a)\left[\frac{(l-1)z}{l-z}\right]^{\frac{1}{2}} + a \quad \text{and} \quad a = \frac{(l-e)^{\frac{1}{2}} - (l-1)^{\frac{1}{2}} e^{\frac{1}{2}}}{(l-e)^{\frac{1}{2}} + (l-1)^{\frac{1}{2}} e^{\frac{1}{2}}},$$

the z-plane outside the slit $(0,0)$ to $(l,0)$ is mapped onto the upper half of the ζ-plane external to the unit circle (figure 4). The wetted-parts of the slit sides map onto the semicircle, $\zeta = e^{i\theta}$, $0 \leqslant \theta \leqslant \pi$, with the point-to-point correspondence $$x^{\frac{1}{2}}/(l-x)^{\frac{1}{2}} = \pm b^{-1}(\cos\theta - a), \quad b = (1+a)(l-1)^{\frac{1}{2}}.$$

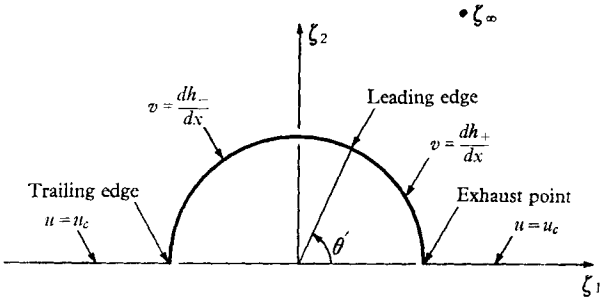

FIGURE 4. Boundary-value problem in upper half of circle plane.

The exhaust point is at $\theta = 0$, the leading edge at $\theta = \theta' = \cos^{-1} a$ and the trailing edge at $\theta = \pi$. The upper and lower free-streamlines map onto $\zeta = \zeta_1$, $|\zeta_1| > 1$ with cavity termination at $\zeta_1 = +\infty$ for the upper free-streamline and at $\zeta_1 = -\infty$ for the lower. The wake maps onto a curve reaching from $\zeta = 2a + i\infty$ for $x = l$ to $\zeta = \zeta_\infty$ for $x = \infty$, with

$$\zeta_\infty = a + ib + \{(a+ib)^2 - 1\}^{\frac{1}{2}}.$$

Thus the boundary-value problem for $w(\zeta)$ is

$$v(e^{i\theta}) = dh_\pm/dx = H(\theta) \quad (0 \leqslant \theta \leqslant \pi), \tag{6}$$

$$w(\zeta_\infty) = 0, \tag{7}$$

$$u(\zeta_1) = u_c = \tfrac{1}{2}K, \quad |\zeta_1| > 1. \tag{8}$$

Analytic continuation into the lower-half ζ-plane shows that

$$w(\zeta) - u_c = -[\overline{w}(\zeta) - u_c],$$

and thus the mixed boundary-value problem for $w(z)$ has been converted into an ordinary type for $w(\zeta)$ with

$$v(e^{i\theta}) = H(\theta), \quad -\pi \leqslant \theta \leqslant \pi, \quad H(-\theta) = H(\theta). \tag{6'}$$

The unknown constant u_c in (8) will be determined by (7).

The closure singularity function in the ζ-plane is $iC(\zeta - \zeta^{-1})$, which, for real C, leaves unaffected the unit-circle and real-axis boundary conditions. Thus (5) shows that the resultant behaviour of $w(z)$ near the cavity termination point is

$$z \to (l,0), \quad w(z) = -C_z(z-l)^{-\frac{1}{2}} + O(1), \tag{9}$$

with $$C_z = 2l^{\frac{1}{2}} bC.$$

Therefore, on the free-streamlines approaching the cavity termination, $v_\pm \to \mp\infty$ if C is positive, and $v_\pm \to \pm\infty$ if C is negative. Proper closing action requires that C be positive, either because the wake otherwise is thicker than the cavity, which is considered inappropriate, or because the implied free-streamlines otherwise cross somewhere before cavity termination, as discussed later.

The above conversion from a mixed to the ordinary type of boundary-value problem would not apply for the case of two cavities, as, for example, with a short vapour cavity near the leading edge, ahead of the main cavity. In such cases, a simple mapping of the sides of the z-plane singularity slit onto the entire real axis gives the type of problem considered by Cheng & Rott (1954), with u and v prescribed on alternate portions of the real axis.

The mapping used here for the case of a single cavity is convenient because of the reduction to the well-known boundary-value problem for the unit circle, but it does not apply directly for $e < l < 1$. On the other hand, a mapping applicable for all l is that used by Woods (1953) in treating the separated boundary-layer problem for $e < l < 1$ or $l = \infty$, whereby the z-plane outside the singularity slit is mapped onto an infinite strip with the wetted surface on one side and the free-streamline on the other.

3. Drag, lift and moment

An advantage of the cavity-termination models selected is that pressure distributions are not needed to obtain drag, lift and pitching moment. Because of the properties of analytic functions, the required pressure-distribution integrations reduce to the calculation of certain key solution parameters. Only the resultant relations are given here. Considering first C_L and C_M, since the pressures along $y = 0\pm$ are equal everywhere off the foil, the hydrofoil lift and moment are the same as on the pseudo-hydrofoil represented by the hydrofoil plus cavity plus wake. For unit chord, with the moment about the leading edge measured clockwise, we have

$$C_L = 4\pi b_1, \quad C_M = -4\pi b_2, \tag{10}$$

where, for $l < \infty$, the solution has the form

$$z \to \infty, \quad w(z) = \frac{a_1 + ib_1}{z} + \frac{a_2 + ib_2}{z^2} + \ldots. \tag{11}$$

In contrast, the form drag does involve the cavity in one way or another. For the open model, the pseudo-hydrofoil is seen to have zero-form drag, and simple considerations show that the hydrofoil's drag coefficient for unit chord is therefore

$$C_D = t_{w_o} K = 2\pi a_{1_o} K, \tag{12}$$

where t_{w_o} is the open-model wake thickness. For the closed model, the net zero drag of the closed pseudo-hydrofoil shows that the hydrofoil drag is balanced by the negative point drag at the cavity termination, as in figure 3, so that (Wu 1957)

$$C_D = 2\pi C_z^2. \tag{13}$$

Possible leading-edge point-drag or suction forces are included in these drag formulas (Jones & Cohen 1960). The relations for C_L, C_M and C_D for the partly closed models are given later.

As will be shown, for every l of interest and for $e \neq 1$, there exists an angle of attack α^+ for which t_w must be zero, so that the cavity has cusp closure, making $C_D = 0$. For $\alpha = \alpha^+$, the open, partly closed and closed models for each l are identical, and for $\alpha < \alpha^+$, each implies improper doubly covered flow, since the implied free-streamlines must cross, as shown in figure 5 for the closed model. For each l, the α^+ and associated u_c^+, C_L^+ and C_M^+ are key parameters common to the three models.

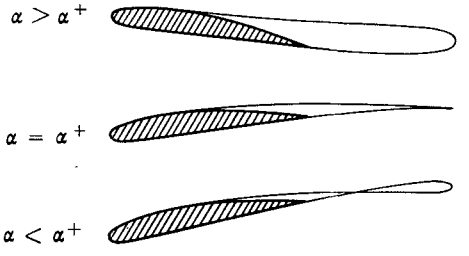

FIGURE 5. Cavity configurations according to angle of attack for closed-cavity model.

For the open-model solution, it is convenient to separate $w_o(z)$ into the cusp-closure solution $w^+(z)$ and $(\alpha-\alpha^+)P(z)$, where $P(z)$ is the $w(z)$ for the *open*-model, flat-plate case for unit angle of attack. From (10), (11) and (12), one has

$$z \to \infty, \quad w^+(z) = \frac{i(C_L^+/4\pi)}{z} + \frac{a_2^+ - i(C_M^+/4\pi)}{z^2} + \ldots \tag{14}$$

and

$$z \to \infty, \quad P(z) = \frac{(t_{w_P}/2\pi) + i(C_{L_P}/4\pi)}{z} + \frac{a_{2_P} - i(C_{M_P}/4\pi)}{z^2} + \ldots, \tag{15}$$

so that the open-model relations for given l are

$$\left.\begin{aligned} \tfrac{1}{2}K = u_c^+ + (\alpha-\alpha^+)\,u_{c_P}, \quad t_{w_o} = (\alpha-\alpha^+)\,t_{w_P}, \\ C_D = t_{w_o}K, \quad C_L = C_L^+ + (\alpha-\alpha^+)\,C_{L_P}, \quad C_M = C_M^+ + (\alpha-\alpha^+)\,C_{M_P}. \end{aligned}\right\} \tag{16}$$

For the closed-model solution, $w_{cl}(z)$, the similar resolution is into $w^+(z)$ and $(\alpha-\alpha^+)Q(z)$, where $Q(z)$ is the $w(z)$ for the *closed*-model, flat-plate case for unit angle of attack. With the expansions

$$z \to \infty, \quad Q(z) = \frac{i(C_{L_Q}/4\pi)}{z} + \frac{a_{2_Q} - i(C_{M_Q}/4\pi)}{z^2} + \ldots \tag{17}$$

and, from (9) and (13),

$$z \to (l, 0), \quad Q(z) = -\{C_{D_Q}/2\pi(z-l)\}^{\frac{1}{2}} + O(1), \tag{18}$$

the closed-model relations for given l are

$$\left.\begin{aligned} \tfrac{1}{2}K = u_c^+ + (\alpha-\alpha^+)\,u_{c_Q}, \quad C_D = (\alpha-\alpha^+)^2 C_{D_Q}, \\ C_L = C_L^+ + (\alpha-\alpha^+)\,C_{L_Q}, \quad C_M = C_M^+ + (\alpha-\alpha^+)\,C_{M_Q}. \end{aligned}\right\} \tag{19}$$

A partly-closed model solution exists, for each given profile, cavity length and angle of attack ($\alpha > \alpha^+$), for each ratio of wake thickness to open-model wake thickness. The solution for each $T = t_w/t_{w_o}$ in the allowable range $0 \leqslant T \leqslant 1$ is

$$w = w^+ + (\alpha-\alpha^+)\,[TP + (1-T)\,Q] = Tw_o + (1-T)\,w_{cl}. \tag{20}$$

Clearly one has $K = TK_o + (1-T)K_{cl}$ plus similar forms for C_L and C_M. The drag integral gives

$$C_D = KT(\alpha-\alpha^+)t_{w_P} + (1-T)^2(\alpha-\alpha^+)^2 C_{D_Q},$$

and the relations between the open- and closed-model flat-plate solutions reduce this to

$$C_D = TC_{D_o} + (1-T)C_{D_{cl}}.$$

Thus for the partly closed model, C_D, C_L, C_M and K for each l and T are obtained from the open and the closed model values by the common relation

$$(\ )_T = T(\ )_o + (1-T)(\ )_{cl}. \tag{21}$$

4. Open-model, smooth-entry solution

While the cusp-closure solution is a natural reference for both the open and closed models, a particular open-model solution w_s, giving 'smooth entry', i.e. no leading-edge suction, is convenient in obtaining the cusp-closure solution. The function $w_s(\zeta)$ is regular outside the unit circle and satisfies

$$-\operatorname{Im}[w_s(e^{i\theta})] = H(\theta) - \alpha_s, \tag{22}$$

$$w_s(\zeta_\infty) = 0, \tag{23}$$

$$\operatorname{Re}[w_s(\zeta_1)] = u_{c_s}, \quad |\zeta_1| > 1, \tag{24}$$

where α_s is the open-model, smooth-entry angle of attack and u_{c_s} the corresponding u_c. Having $w_s(\zeta)$, $w^+(\zeta)$ is readily obtained from

$$w^+(\zeta) = w_s(\zeta) + (\alpha^+ - \alpha_s)P(\zeta),$$

where α^+ is to be determined by the condition $t_w^+ = 0$. Thus with

$$z \to \infty, \quad w_s(z) = \frac{(t_{w_s}/2\pi) + i(C_{L_s}/4\pi)}{z} + \frac{a_{2_s} - i(C_{M_s}/4\pi)}{z^2} + \ldots; \tag{25}$$

then, except for $e = 1$ (for which $t_{w_P} = 0$), $\alpha^+ - \alpha_s$ exists, given by

$$\alpha^+ - \alpha_s = -a_{1_s}/a_{1_P} = -t_{w_s}/t_{w_P}, \tag{26}$$

and the cusp-closure parameters are seen to be

$$u_c^+ = u_{c_s} - (t_{w_s}/t_{w_P})u_{c_P}, \quad C_L^+ = C_{L_s} - (t_{w_s}/t_{w_P})C_{L_P}, \quad C_M^+ = C_{M_s} - (t_{w_s}/t_{w_P})C_{M_P}. \tag{27}$$

Because the smooth-entry solution cannot have leading-edge suction, the only singularities in $w_s(e^{i\theta})$ are those due to discontinuities or singularities in $H(\theta)$. The function $w_s(\zeta)$ is obtained as follows. Let

$$w_s' = i[w_s(\zeta) - (u_{c_s} + i\alpha_s)],$$

so that w_s' is the analytic function regular outside the unit circle with its real part thereon equal to $H(\theta) = H(-\theta)$ and with its imaginary part zero on $\zeta = \zeta_1$, $|\zeta_1| > 1$. Thus $w_s'(\Omega)$, where $\Omega = 1/\zeta$, is seen to satisfy the boundary conditions of Boggio's formula, so that (Bateman 1944)

$$w_s'(\Omega) = \frac{(1-\Omega^2)}{\pi}\int_0^\pi \frac{H(\phi)\,d\phi}{1 - 2\Omega\cos\phi + \Omega^2}.$$

Therefore

$$w_s(\zeta)-(u_{c_s}+i\alpha_s)=-\frac{i(\zeta^2-1)}{\pi}\int_0^\pi \frac{H(\phi)\,d\phi}{\zeta^2-2\zeta\cos\phi+1}, \tag{28}$$

and, from (23),

$$u_{c_s}+i\alpha_s=\frac{i(\zeta_\infty^2-1)}{\pi}\int_0^\pi \frac{H(\theta)\,d\theta}{\zeta_\infty^2-2\zeta_\infty\cos\theta+1}.$$

The equivalent power series is (Kellogg 1929)

$$w_s(\zeta)=u_{c_s}+i\alpha_s-i\sum_0^\infty c_n\zeta^{-n}, \tag{29}$$

with $$c_0=\frac{1}{\pi}\int_0^\pi H(\theta)\,d\theta, \quad c_n=\frac{2}{\pi}\int_0^\pi H(\theta)\cos n\theta\,d\theta \quad (n\neq 0)$$

and $$u_{c_s}+i\alpha_s=i\sum_0^\infty c_n\zeta_\infty^{-n}.$$

The major complication of finite cavity length is simply that $w_s(\zeta)$ and its first two derivatives must be evaluated at $\zeta_\infty \neq \infty$, so that the appropriate power series no longer reduce to simple polynomials. For large $|\zeta_\infty|$, i.e. large l, the power series can be approximated by their first few terms, as was done for $e=0$ by Wu (1956). However, short cavity lengths are commonly of interest for forced venting when α is near α^+, because then drag is low and hence the cavity length shortens rapidly as K increases. Thus the integral solution is emphasized here.

The required parameters of $w_s(\zeta)$ are obtained as follows. Letting $Z=1/z$, then

$$\frac{t_{w_s}}{2\pi}+i\frac{C_{L_s}}{4\pi}=\left.\frac{dw_s}{dZ}\right|_0=\left.\frac{dw_s}{d\zeta}\right|_{\zeta_\infty}\left.\frac{d\zeta}{dZ}\right|_0, \tag{30}$$

and $$a_{2_s}-i\frac{C_{M_s}}{4\pi}=\frac{1}{2}\left.\frac{d^2w_s}{dZ^2}\right|_0=\frac{1}{2}\left[\left.\frac{d^2w_s}{d\zeta^2}\right|_{\zeta_\infty}\left(\left.\frac{d\zeta}{dZ}\right|_0\right)^2+\left.\frac{dw_s}{d\zeta}\right|_{\zeta_\infty}\left.\frac{d^2\zeta}{dZ^2}\right|_0\right]. \tag{31}$$

Because C_M is appreciably more laborious to calculate, it is not considered further here. The mapping $\zeta(z)$ shows that, using $\zeta_\infty=\Lambda e^{i\lambda}$ and $\zeta_\infty-a-ib=Ne^{i\nu}$,

$$\left.\frac{d\zeta}{dZ}\right|_0=\tfrac{1}{2}ibl\left(\frac{\Lambda e^{i\lambda}}{N e^{i\nu}}\right). \tag{32}$$

The key relations are found from (28) and (30) to be

$$u_{c_s}+i\alpha_s=\frac{1}{\pi}\int_0^\pi[\Lambda G+\tfrac{1}{2}i(\Lambda^2-1)F]H\,d\theta, \tag{33}$$

$$\frac{t_{w_s}}{2\pi}+i\frac{C_{L_s}}{4\pi}=\frac{bl\,e^{-i\nu}}{2N}\left\{\frac{1}{\pi}\int_0^\pi[\Lambda G+\tfrac{1}{2}i(\Lambda^2-1)F]^2H\,d\theta - \frac{[2\Lambda^2\sin 2\lambda+i(\Lambda^4-1)]}{(\Lambda^4+1-2\Lambda^2\cos 2\lambda)}(u_{c_s}+i\alpha_s)\right\}, \tag{34}$$

where $$F=\frac{1}{\Lambda^2+1-2\Lambda\cos(\lambda+\theta)}+\frac{1}{\Lambda^2+1-2\Lambda\cos(\lambda-\theta)},$$

$$G=\frac{\sin(\lambda+\theta)}{\Lambda^2+1-2\Lambda\cos(\lambda+\theta)}+\frac{\sin(\lambda-\theta)}{\Lambda^2+1-2\Lambda\cos(\lambda-\theta)}.$$

These relations follow from the identity

$$\frac{\zeta_\infty^2-1}{\zeta_\infty^2-2\zeta_\infty\cos\theta+1}=\frac{1}{2}\left(\frac{\zeta_\infty+e^{i\theta}}{\zeta_\infty-e^{i\theta}}+\frac{\zeta_\infty+e^{-i\theta}}{\zeta_\infty-e^{-i\theta}}\right)=-i[\Lambda G+\tfrac{1}{2}i(\Lambda^2-1)F].$$

Because of the complexity of (33) and (34), it is important to make maximum use of basic solutions constructed from unit-circle singularities. The flat-plate solutions are of this type and, as seen earlier, are also necessary in the consideration of angle of attack.

5. Vented flat plate

The open-model solution $P(\zeta)$ for the vented flat plate is obtained by placing the leading-edge singularities of fully wetted flow (Biot 1942) at the leading-edge point, $e^{+i\theta'}$, and its image, $e^{-i\theta'}$, so that for unit angle of attack

$$P(\zeta)=u_{c_P}+i(1-\beta_P)-i\beta_P\left(\frac{e^{i\theta'}}{\zeta-e^{i\theta'}}+\frac{e^{-i\theta'}}{\zeta-e^{-i\theta'}}\right). \tag{35}$$

That the unit-circle and real-axis boundary conditions are satisfied is easily seen. The constants u_{c_P} and β_P are determined by $P(\zeta_\infty)=0$, giving

$$u_{c_P}=\beta_P\left(\frac{a}{b}-\frac{\cos\lambda}{b\Lambda}\right),\quad \frac{1}{\beta_P}=1+\frac{\sin\lambda}{b\Lambda}. \tag{36}$$

From (35) and (32), one obtains

$$(t_{w_P}/2\pi)+i(C_{L_P}/4\pi)=(\beta_P l/2bN)\{[-(1-a^2)\cos\nu+ab\sin\nu] +i[ab\cos\nu+(1-a^2)\sin\nu]\}. \tag{37}$$

Tables of u_{c_P}, t_{w_P} and C_{L_P} for various l and e values ($\infty\leqslant l\leqslant 1$ and $0\leqslant e\leqslant 1$) have been calculated to allow ready treatment of general α and K with the open model. The solid curves in figure 6 show $C_D/\alpha^2=2t_{w_P}u_{c_P}$ and $C_L/\alpha=C_{L_P}$ *vs* $K/2\alpha=u_{c_P}$ for constant e, and the dashed curves are constant-l contours.

To obtain the flat-plate closed-cavity solution $Q(\zeta)$, one adds the closure singularity function so that, with $C=C'\beta_Q$,

$$Q(\zeta)=u_{c_Q}+i(1-\beta_Q)-i\beta_Q\left(\frac{e^{i\theta'}}{\zeta-e^{i\theta'}}+\frac{e^{-i\theta'}}{\zeta-e^{-i\theta'}}\right)+iC'\beta_Q\left(\zeta-\frac{1}{\zeta}\right). \tag{38}$$

The unit-circle and real-axis boundary conditions are unaffected. The zero condition at ζ_∞ yields

$$u_{c_Q}=\beta_Q\left[\frac{u_{c_P}}{\beta_P}+C'\left(\Lambda+\frac{1}{\Lambda}\right)\sin\lambda\right],\quad \frac{1}{\beta_Q}=\frac{1}{\beta_P}-C'\left(\Lambda-\frac{1}{\Lambda}\right)\cos\lambda. \tag{39}$$

Since

$$\left.\frac{dQ}{d\zeta}\right|_{\zeta_\infty}=\beta_Q\left[\frac{1}{\beta_P}\left.\frac{dP}{d\zeta}\right|_{\zeta_\infty}+iC'\left(1+\frac{1}{\zeta_\infty^2}\right)\right],$$

then, parallel to the open-model development, one obtains

$$i\frac{C_{L_Q}}{4\pi}=\beta_Q\left[\frac{1}{\beta_P}\left(\frac{t_{w_P}}{2\pi}+i\frac{C_{L_P}}{4\pi}\right)-C'\left(\zeta_\infty+\frac{1}{\zeta_\infty}\right)\left(\frac{bl}{2N}\right)e^{-i\nu}\right]. \tag{40}$$

C' is determined from (40) using the condition, already implied there, that $t_{w_Q} = 0$. C_{L_Q} follows directly. C_{D_Q} is obtained from (13), using $C_z = 2l^{\frac{1}{2}}bC'\beta_Q$. Using these relations, tables of u_{c_Q}, C_{D_Q} and C_{L_Q} *vs* l and e have also been calculated.

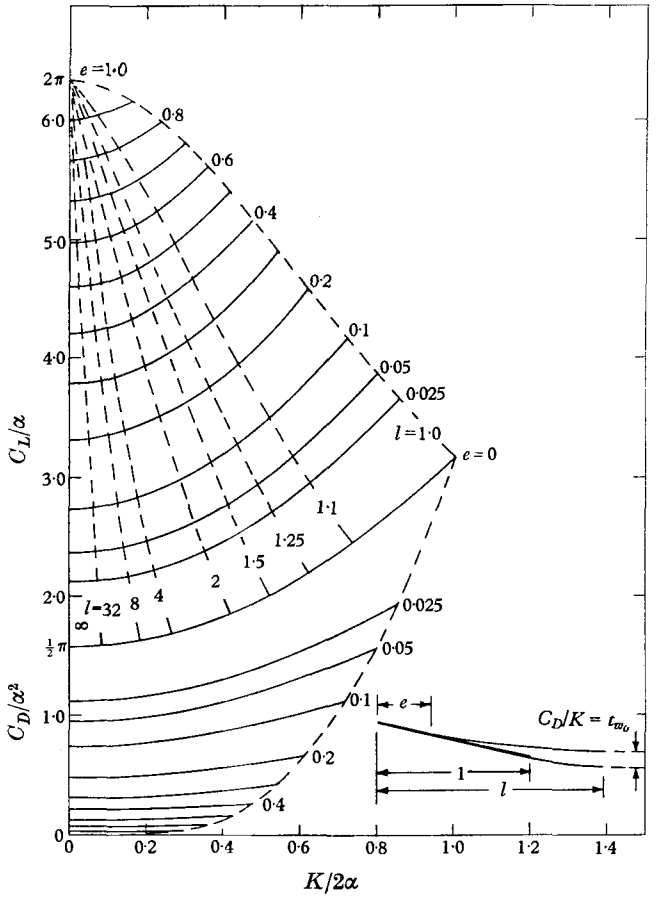

FIGURE 6. Drag, lift, and cavity length *vs* cavity number for vented flat plate for open-cavity model and various exhaust locations.

Figure 7 gives $C_D/\alpha^2 = C_{D_Q}$ and $C_L/\alpha = C_{L_Q}$ *vs* $K/2\alpha = u_{c_Q}$ for constant e and the corresponding closed-model cavity length *vs* $K/2\alpha$ and e. The major difference seen in figures 6 and 7 is the shorter open-model cavity lengths for a given K. It can be shown that the cavity-length ratio $l_o/l_{cl} \to \frac{1}{4}$ as $K \to 0$, which is the same as for trailing edge venting (Fabula 1960). While K for the open model and a given α is finite for $L = 1$ ($K = K_1$), the combination of the partly-closed model family and the closed-model limit, i.e. $0 \leqslant T < 1$, has $K \to \infty$ for $l \to 1$ due to the closure singularity. Thus for each K and α there is a continuous range of possible l values, namely $l_o \leqslant l \leqslant l_{cl}$ if $K \leqslant K_1$, and $1 < l \leqslant l_{cl}$ if $K > K_1$. It is readily seen that such relations also hold for an arbitrary profile in terms of $K - K^+$ and $\alpha - \alpha^+$. For purposes of comparison with experiment, it is interesting to note that the family of cavity termination models employed typically implies

noticeably shorter cavity length if and when wake thickness for unit chord is no longer negligible in comparison with $t_{w_o} = C_{Do}/K \approx C_D/K$, where C_D and K are experimental values.

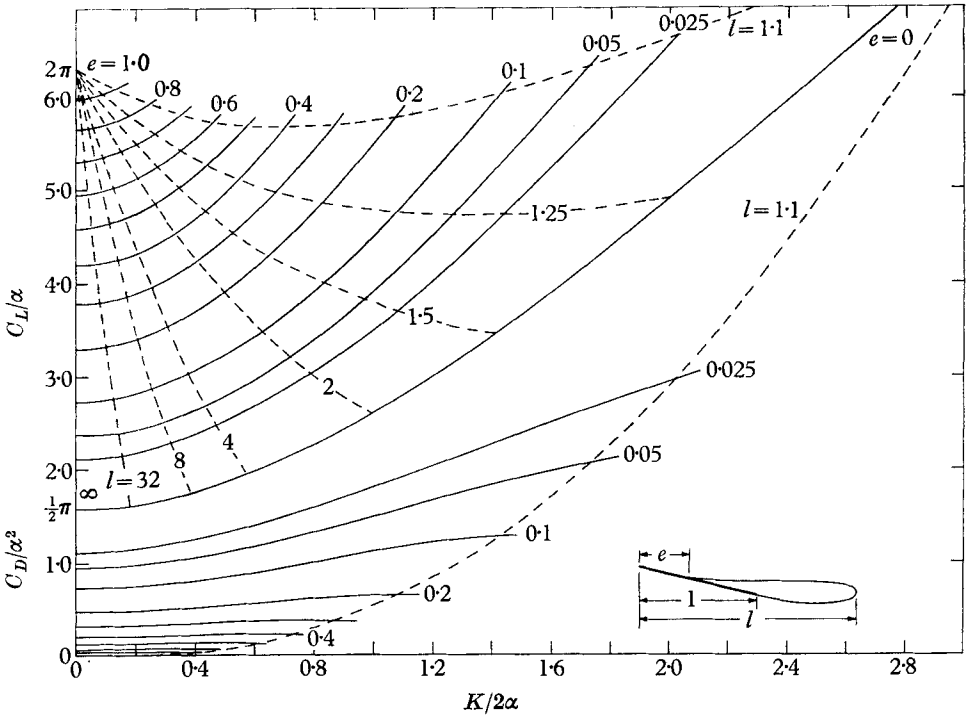

FIGURE 7. Drag, lift, and cavity length *vs* cavity number for vented flat plate for closed-cavity model and various exhaust locations.

6. Other basic profiles

Solutions for other simple profiles and profile components can be constructed from singularities on the unit circle. Examples are cases of piecewise-uniform contour slope corresponding to polygonal profiles, such as the plain flap vented at the hinge and the vented split flap.

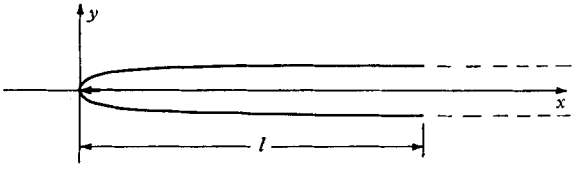

FIGURE 8. Open-model point-drag cavity profile.

With the typical case of a parabolic leading edge with local thickness distribution proportional to $x^{\frac{1}{2}}$, the resultant singularity in H for $\theta \to \theta'$ is removed by use of the open-model, point-drag solution for finite cavity length, as shown in figure 8 (Fabula 1960). The corresponding profile expression is

$$\tilde{h}_{\pm} = \pm \tilde{u}_c l\{x^{\frac{1}{2}}(l-x)^{\frac{1}{2}}/l + \sin^{-1}(x/l)^{\frac{1}{2}}\}, \tag{41}$$

and thus $\tilde{u}_c$, the contribution to u_c for a given l by the point-drag solution, is determined by the leading-edge radius. The contributions to t_w and C_L are clearly

$$\tilde{t}_w = \pi \tilde{u}_c l, \quad \tilde{C}_L = 0. \tag{42}$$

7. A comparison with experiment

In order to make a first fairly complete experimental test of theory, it is desirable to test a vented or cavitating hydrofoil with a simple form over a wide range of cavity numbers. Such a case is the cavitating profile of figure 9 for

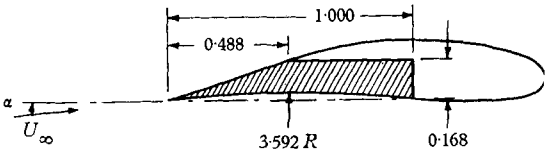

FIGURE 9. Test hydrofoil configuration.

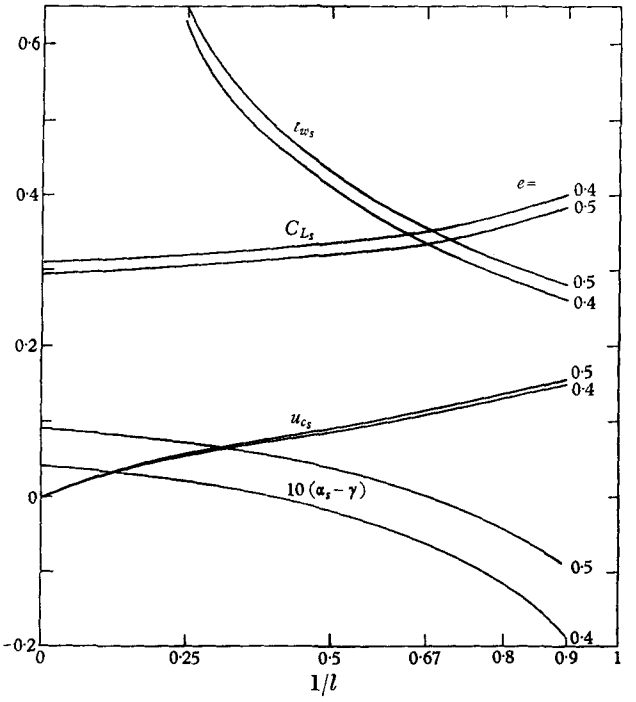

FIGURE 10. Open-model, smooth-entry solution parameters for test hydrofoil (with $e = 0{\cdot}4$ or $0{\cdot}5$ instead of $0{\cdot}488$).

which the cavity configuration shown occurred in a narrow range of angle of attack (obviously near the smooth-entry angle), and for which C_D and C_L data are available for $\alpha = 7°$ and $8°$ with K between about $0{\cdot}2$ and $1{\cdot}0$ (Parkin 1956). The wetted-surface contour slope distribution for the test hydrofoil is conveniently approximated as

$$H(\theta) \approx \gamma + \delta, \quad 0 \leqslant \theta < \theta'; \quad H(\theta) \approx \gamma - 2\gamma x, \quad \theta' < \theta \leqslant \pi; \quad (\gamma = 8°, \delta = 11°).$$

The results of planimeter integration to obtain the open-model, smooth-entry parameters for $e = 0{\cdot}4$ and $0{\cdot}5$ and $l = \infty$, 4, 2, 1·5, 1·25 and 1·1 are given in figure 10.

It is simple to go from the open-model, smooth-entry parameters to the cusp-closure parameters with the tables of the open-model flat-plate parameters. Next, the open- and closed-model C_D, C_L and K *vs* l are easily obtained via the

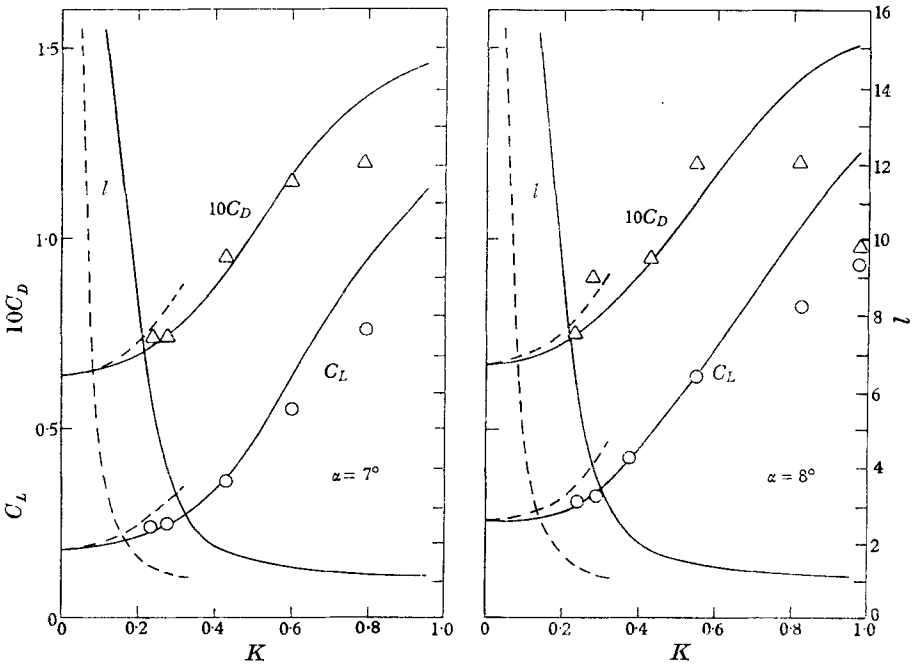

FIGURE 11. Comparison of theoretical and experimental lift and drag *vs* cavity number for the side-cavitated hydrofoil.

respective tables. Figure 11 gives the experimental data and the final theoretical curves of C_D, C_L and l *vs* K for $\alpha = 7°$ and $8°$ and $e = 0{\cdot}49$, obtained by interpolation from the results for $e = 0{\cdot}4$ and $0{\cdot}5$. Solid and dashed curves give closed- and open-model results, respectively. While the open model reaches $l = 1$ for finite K, the closed model has $K \to \infty$ for $l \to 1$. The results for the partly closed model are easily constructed according to the simple relations given earlier. In accord with other comparisons of theory and vapour-cavity experiments, the closed model seems appropriate, but partly closed models for small T would be equally appropriate.

The force comparison is good up to $K \approx 0{\cdot}65$, which is as high a value as that for which one might hope linearized theory to be useful. The experimental C_D-behaviour for $K > 0{\cdot}65$, for which $l_{cl} < 1{\cdot}25$, suggests that the thick trailing edge is being hit by the typical re-entrant jet which is expected to be present to some extent. Unfortunately water-tunnel photographs to check this and to compare cavity lengths are not available.

This work was done as part of an investigation of forced-vented hydrofoils for the Bureau of Naval Weapons, U.S. Navy. Helpful suggestions by Prof. T. Yao-tsu Wu are gratefully acknowledged. The flat-plate parameter tables and a comparison of theory and experiment for two hydrofoils with forced ventilation will be given in a future NAVWEPS report.

REFERENCES

BATEMAN, H. 1944 *Partial Differential Equations of Mathematical Physics*, p. 239. New York: Dover.

BIOT, M. A. 1942 Some simplified methods in airfoil theory. *J. Aero. Sci.* **9**, 185.

CHENG, H. K. & ROTT, N. 1954 Generalizations of the inversion formula of thin airfoil theory. *J. Rat. Mech. Anal.* **3**, 357.

FABULA, A. G. 1960 Application of thin airfoil theory to hydrofoils with cut-off ventilated tailing edge. *Nav. Ord. Test Sta. NAVWEPS Rep.* no. 7571.

JONES, R. T. & COHEN, DORIS 1960 *High Speed Wing Theory*, p. 23. Princeton University Press. (See also Vol. VII of *High Speed Aerodynamics and Jet Propulsion*, Princeton University Press.)

KELLOGG, O. M. 1929 *Foundations of Potential Theory*, p. 353. Berlin: Springer Verlag.

LANG, T. G. 1959 Base-vented hydrofoils. *Nav. Ord. Test Sta. NAVORD Rep.* no. 6606.

LANG, T. G., DAYBELL, D. A. & SMITH, K. E. 1959 Water-tunnel tests of hydrofoils with forced ventilation. *Nav. Ord. Test Sta. NAVORD Rep.* no. 7008.

PARKIN, B. R. 1956 Experiments on circular arc and flat plate hydrofoils in noncavitating and full cavity flows. *Calif. Inst. Tech. Hydro. Lab. Rep.* no. 47–6.

THWAITES, B. (Ed.) 1960 *Incompressible Aerodynamics.* Oxford University Press.

TULIN, M. P. 1953 Steady two-dimensional cavity flows about slender bodies. *David Taylor Model Basin Rep.* no. 834.

WOODS, L. C. 1953 Theory of aerofoils on which occur bubbles of stationary air. *Aero. Res. Counc., Lond., Rep. & Mem.* no. 3049.

WU, T. YAO-TSU 1955 A free streamline theory for two-dimensional fully cavitated hydrofoils. *Calf. Inst. Tech. Hydro. Lab. Rep.* no. 21–17.

WU, T. YAO-TSU 1956 A note on the linear and nonlinear theories for fully cavitated hydrofoils. *Calif. Inst. Tech. Hydro. Lab. Rep.* no. 21–22.

WU, T. YAO-TSU 1957 *A simple method for calculating the drag in the linear theory of cavity flows. Calif. Inst. Tech. Engng Div. Rep.* no. 85–5.